A comparison of linear and nonlinear energy calculations for long-crested surface waves

Baddour, R. E.; Parsons, W.

13th Annual Conference on Computational and Fluid Dynamics [Proceedings], 2005

A Comparison of Linear and Nonlinear Energy Calculations for Long-crested Surface Waves

W. Parsons[1] and E. Baddour[2*]
[1]College of North Atlantic
Ridge Road Campus, St. John's, NL, A1C 6L8, Canada
[2]National Research Council
Institute for Ocean Technology, St. John's, NL, A1B 3T5, Canada

Email: *Emile.Baddour@nrc.ca*

Abstract

This paper compares the energy calculations of the potential and kinetic energy, and the power generated by a gravity water wave, using fully nonlinear theory with the corresponding calculations using simple linear theory. To perform these nonlinear calculations a fully nonlinear numerical wave-tank model is utilized to generate and propagate monochromatic gravity long-crested waves for an incompressible invicid homogeneous fluid of infinite depth. This model employs a non-orthogonal curvilinear coordinate system, which follows the free surface so the entire fluid domain contributes to the energy calculations at all times and up to the free surface.

1 Introduction

A two-dimensional rectangular basin containing an incompressible inviscid homogeneous fluid initially at rest with a horizontal free surface of finite extent is considered to generate and propagate long-crested waves. On the left vertical boundary a wavemaker is positioned while at the right hand side is the radiation boundary. The same numerical beach is used as in [1], and a depth profile for the potential is assumed, giving us a waveform relaxation method, and thereby drastically reducing the computational cost of solving Laplace's equation. A monochromatic deterministic wavemaker employing a Diriclet type boundary condition is applied, see [2]. This method can easily be extended to the case of a wavemaker utilizing a Neumann type boundary condition see [2]. Laplace's equation is solved using a non-orthogonal curvilinear coordinate system, which follows the free surface. This gives a more realistic "continuity condition", since it involves the entire fluid domain. Also, the full nonlinear kinematic and dynamic free surface boundary conditions are employed. Although, these ideas can be extended to finite depth tanks, we restrict our attention to the infinite depth case. In this paper, we use the evolution of regular, monochromatic nonlinear steep, long-crested waves in the numerical basin to compute their average energy content. The energy calculations are performed up to the free surface as provided by the simulation hence satisfying the nonlinear conditions. Comparison with the standard energy computations (to O(H^2)) for first order waves where H is the wave height, is provided. The steepness of the wave system affects the computation of its wave energy content.

2 Standard linear ocean waves energy content estimation

The standard linear ocean energy content estimations is available in most water wave mechanics textbooks; in particular see [3]. For convenience, we give the equations with some explanation and discussion. The total energy, E in the wave consists of potential energy, PE, which results from displacing the mass of fluid in the wave from a position of equilibrium against a gravitational field and the kinetic energy, KE associated with the motion of the water. Since these quantities continually change with position and time, one usu-

*Corresponding author

ally averages the total energy over one wavelength. In addition, this average is taken per unit surface area associated with the wave. In this report, where possible, we employ the notation used in the papers [2] and [4] . We consider the two-dimensional infinite depth case of long crested deep waves, and assume that we have an incompressible inviscid homogeneous fluid of constant (area) density ρ, in a Cartesian coordinate system (x, z), with the origin at the still water level and the positive z-axis pointing upwards. See Figure 1 in [4].

Assume the existence of a fully formed travelling sinusoidal wave,

$$\eta(x,t) = (H/2)\cos(kx - \omega t) \tag{1}$$

where H is the wave height, and k and ω the wavenumber and angular frequency, respectively, and recall the standard infinite depth dispersion relation

$$\omega = \sqrt{gk}, \tag{2}$$

where the wavelength, λ and the period, T, are related to the wavenumber, k and the angular frequency, ω, as follows:

$$\lambda = \frac{2\pi}{k}, \text{ and } T = \frac{2\pi}{\omega}. \tag{3}$$

Since we are looking at the infinite depth case, we define $z = -h$ to be some convenient reference depth, usually around a wavelength. Then the total potential energy $\overline{PE}_T$, with and without waves, averaged over one wavelength λ, relative to $z = -h$, is given by the following integration

$$\overline{PE}_T = \frac{1}{\lambda}\int_x^{x+\lambda} \rho g \frac{(h+\eta)^2}{2} dx, \tag{4}$$

where g is the acceleration due to gravity. Since we are integrating a simple **single** sinusoid, given by Equation (1), and we are averaging over a **complete** wavelength, this integral simplifies to

$$\overline{PE}_T = \rho g \frac{h^2}{2} + \rho g \frac{H^2}{16}. \tag{5}$$

This expression contains two terms, the potential energy without and with waves, so $\overline{PE}$, the potential energy of the wave, given by Equation (1), averaged over one wavelength, per unit surface area is

$$\overline{PE} = \rho g \frac{H^2}{16}. \tag{6}$$

Similarly the average kinetic energy per unit surface area must be integrated over depth and averaged over wavelength. If u and v represent the x and z components of velocity, respectively, then this average kinetic energy, $\overline{KE}$ is given by the double integral

$$\overline{KE} = \frac{1}{\lambda}\int_x^{x+\lambda}\int_{-h}^{\eta=0} \rho \frac{u^2 + w^2}{2} dz dx. \tag{7}$$

Assuming the conditions for potential flow are satisfied (no wave breaking, for example), we can use standard linear theory to write the potential

$$\Phi(x,z,t) = \frac{Hg}{2\omega} e^{kz} \sin(kx - \omega t), \tag{8}$$

so

$$u = \frac{\partial \Phi}{\partial x} = \frac{H\omega}{2} e^{kz}\cos(kx - \omega t), \tag{9}$$

$$w = \frac{\partial \Phi}{\partial z} = \frac{H\omega}{2} e^{kz}\sin(kx - \omega t), \tag{10}$$

where we have used the linear dispersion relation, Equation (2). Substituting Equations (9) and (10) into Equation (7), and integrating only up to the still water level, $\eta = 0$, (therefore assuming that the waves have "small"amplitude), we get

$$\overline{KE} = \frac{\rho g H^2}{16}\left(1 - e^{-2kh}\right). \tag{11}$$

Combining this with Equation (6), the total energy, $\overline{E}$ per unit surface area averaged over wavelength is

$$\overline{E} = \overline{PE} + \overline{KE} = \frac{\rho g H^2}{16}\left(2 - e^{-2kh}\right). \tag{12}$$

Note that if the reference level $h \to \infty$, then the Equations (11) and (12), becomes the standard Equations,

$$\overline{KE} = \frac{\rho g H^2}{16}, \tag{13}$$

and

$$\overline{E} = \frac{\rho g H^2}{8}, \tag{14}$$

for infinite depth waves. If a "hyperbolic" depth profile is assumed in Equation (8) for the finite depth case, we also get this same result, Equation (14); see [3].

3 Non-standard nonlinear ocean energy estimation

Our approach will be to employ the full nonlinear numerical model developed by Baddour and Parsons and solve directly and numerically the integrations in Equations (4) and (7), where, for the latter equation, we perform the integration up to the free surface, η, which is conveniently available in our model, since we employ a "boundary fitted" curvilinear coordinate system which tracks the free surface. We refer the reader to the three papers by Baddour and Parsons.

The general algorithm consists of evaluating the integrations:

$$\overline{PE} = \frac{1}{\widetilde{\lambda}} \int_{x}^{x+\widetilde{\lambda}} \rho g \frac{(h+\eta)^2}{2} dx - \rho g \frac{h^2}{2}, \tag{15}$$

$$\overline{KE} = \frac{1}{\widetilde{\lambda}} \int_{x}^{x+\widetilde{\lambda}} \int_{-h}^{\eta} \rho \frac{u^2+w^2}{2} dz dx, \tag{16}$$

$$\overline{E} = \overline{PE} + \overline{KE}, \tag{17}$$

where $\widetilde{\lambda}$ is a "representative" wavelength, appropriate to the wave system under consideration. For a single pure sinusoid, it is just the wavelength, λ, but for the numerical wave generated by the model, it will be taken as the distance between successive "zero-upcrossings" or successive "zero-downcrossings". Since the most energetic waves are steep waves, we are interested in steep finite amplitude waves of steepness $S = H/\lambda$, where H represents the wave height. Also, a large part of the energy available for extraction will be "lost" if the wave breaks, so we are interested in steep waves, "just before breaking". Therefore we may apply Potential Theory to calculate the velocity flow-field; recall that

$$u = \frac{\partial \Phi}{\partial x}, \ w = \frac{\partial \Phi}{\partial z}. \tag{18}$$

Since the waves are steep, the full nonlinear treatment is essential and the "small amplitude" assumption, $\eta = 0$, utilized in Equations (7) is violated, requiring the integration in Equation (16) to be taken " all the way up to η", as indicated in the equation.

The algorithm performs the integrations numerically in Equations (15) and (16) to calculate the potential energy, the kinetic energy, respectively, and therefore the total energy. A vector containing the discretized free surface elevation, η for the representative wavelength, $\widetilde{\lambda}$, and a matrix containing the corresponding discretized potential, along with other necessary parameters is input to a MATLAB program from the numerical wavetank model. A combination of cubic spline interpolation and the MATLAB code **QUAD8**, which employs an adaptive recursive Newton-Cotes 8 panel quadrature method, with a default tolerance of 1×10^{-3} performs all integrations. In addition, the velocity flow field needed in Equation (16), is developed by numerically evaluating the derivatives in Equation (18); again using cubic splines.

4 The numerical wavetank model used

A two-dimensional rectangular basin of infinite depth containing an incompressible inviscid homogeneous fluid initially at rest with a horizontal free surface of finite extent is considered to generate and propagate long-crested waves. A monochromatic deterministic wavemaker employing a Dirichlet type boundary condition is applied at the left hand side of the tank, see [4], and a numerical beach is applied to the right hand side; see [1]. Laplace's equation is solved using second-order finite differences on a non-orthogonal curvilinear coordinate system, which follows the free surface and the full nonlinear kinematic and dynamic free surface boundary conditions are satisified. An assumed depth profile for the potential forms the "first guess" in the iterative waveform relaxation method which reduces the computation dimension of Laplace's equation by one. The starting values for the time integration are calculated using a forth-order explicit Runge-Kutta method after which, a fourth-order Adams predictor-corrector method is used; cubic splines are again used to evaluate all numerical derivatives needed in the time integration, see [4] for the details.

5 Comparison of linear and nonlinear energy calculation

Our procedure for computing the nonlinear energy estimate will be to run our fully nonlinear numerical wavetank model with a monochromatic wavemaker, and study the energy content of the waves generated in the tank by the action of this wavemaker. In this way, we can input waves and their associated velocity fields (given by the potential) using **standard known linear** theory, yet have **fully nonlinear** waves and their associated velocity fields to study.

The reporting of the results of the tests are given in the tables below. These tables give the wave steepness, S at the wavemaker and wave height, H of the wave under consideration. Representative plots in Figure (1) and (2) contains the free surface elevation, η along the length, x of the tank, after a typical simulation time, usually expressed in terms of the wavemaker period, T. Figure (1) is representative of a linear case while Figure (2) presents the free surface profile of a nonlinear simulation. The plot show the typical wavelength over which the nonlinear average energy calculations are performed The linear case takes the wave height H, the wavelength, λ, and the period T of the wavemaker as it's parameters. The (linear) energy estimate, then, uses Equations (6) and (13) to calculate $\overline{PE}$ and $\overline{KE}$, respectively. The associated average power $\overline{P}$ is given by $P = \overline{E}/T$, where we recall that $\overline{E}$ is the total energy, per unit surface area averaged over a representative wavelength λ, and $\overline{E}$ is always the sum of $\overline{PE}$ and $\overline{KE}$.

For the nonlinear calculation we select a representative wavelength, $\widetilde{\lambda}$, which is defined as the distance between successive zero-upcrossings or successive zero-downcrossings. These wavelengths are numbered in the table, $\lambda_1, \lambda_2, \cdots$, and are indicated directly in the plot as shown in Figure (2). The numerical wavetank contains a vector η, of free surface elevations over the length of the tank, $0 \leq x \leq L$, and it contains a matrix, Φ, the associated potential over the total (computational) fluid domain, $0 \leq x \leq L, -h < z \leq \eta(x, N * \widetilde{T})$, where the total simulation time is for "N" (usually a natural number) periods of the wavemaker. Based on the selected wavelength λ_i, we can select a subset of η and a subset of Φ associated with λ_i. Then, $\overline{PE}$, $\overline{KE}$,$\overline{E}$ and $\overline{P}$ can be calculated using the numerical model, along with the representative period $\widetilde{T}$.

We run our numerical wavetank model with a monochromatic wavemaker using the following parameters. The length of the numerical wavetank, $L = 1.0m$, the wavenumber, $k = 25.133(1/m)$ the angular frequency, $\omega = 15.702(1/s)$, the amplitude, $A = 0.00125(m)$ and the wave height, $H = 0.00250(m)$. Therefore the wavelength, $\lambda = 0.25m$ and the steepness, $S = 0.01$. This is a "small amplitude wave" and therefore we expect the nonlinear energy calculations to be "very close" to the linear energy calculations given by Equation (12). This is expected and is therefore a major validation criterion for our algorithm, since, for small steepness waves, the approximation $\eta = 0$ used in the integration in Equation (7) is quite good, and the free surface elevation η and it's associated potential Φ generated by the nonlinear model are "very close" to the respective η and Φ from the linear model; Equations (1) and (8). Note that for the linear calculation, $\overline{PE} = \overline{KE}$; this is characteristic for conservative (nondissipative) systems. See [3].

To tabulate the differences between the nonlinear energy calculations and the linear calculations, we perform further tests with steepness values,

$$S = H/\lambda = 0.2, 0.3, 0.4, 0.5, 0.6 \text{ and } 0.7. \quad (19)$$

As the steepness increases, the difference between our nonlinear energy calculation and the linear calculation will increase, as the above two assumptions in the linear calculations become more suspect. For all of these tests, we keep other parameters fixed. The discretization parameters are $\Delta x = \lambda/20$, $\Delta z = \lambda/10$ and $\Delta t = T/20$, where $T = 0.400(s)$ is the period and is given by Equation (3), and we perform the simulation from "still water" initial conditions for 10 periods, i.e. $10T$. We note that since we passed the vector η and the matrix Φ directly from the numerical wavetank model to the energy model, and since none of the tests involved an increase in the number of points used in the energy algorithm, the discretization parameters for the numerical wavetank model and the discretization parameters for the energy model are the same. Finally $h = \lambda$, where, λ is given by Equation (3).

In Tables 1 and 2 we run the numerical wavetank model for small amplitude waves and, as expected, the linear and nonlinear energy estimates are similar, especially for the $S = 0.01$ case, in Table 1; the $S = 0.02$ case, in Table 2 shows a larger difference. Interestingly, the nonlinear energy estimate, in the λ_1 and λ_2 cases show a **greater** energy estimate than the linear case estimate. Since, λ_3 is closer to the numerical beach, we expect the energy estimate associated with it to be lower. In the tables below the average energy $\overline{E}$ and average power $\overline{P}$ for a unit of surface area of water waves are given in milli-Joule per m of wave length and per m of wave crest i.e. milli-Joule/ m^2 and milli-Watt / m^2 , respectively. The wave length $\widetilde{\lambda}$ and period $\widetilde{T}$ are in m and s, respectively.

Table 1: $S = 0.01$, $H = 0.0025m$

Type	$\widetilde{\lambda}$	$\overline{E}$	$\widetilde{T}$	$\overline{P}$
linear	0.250	7.664	0.400	19.2
λ_1	0.240	7.926	0.392	20.2
λ_2	0.242	7.887	0.393	20.1
λ_3	0.248	7.271	0.399	18.2

Table 2: $S = 0.02$, $H = 0.0050m$

Type	$\widetilde{\lambda}$	$\overline{E}$	$\widetilde{T}$	$\overline{P}$
linear	0.250	30.66	0.400	76.6
λ_1	0.241	31.25	0.393	79.6
λ_2	0.242	31.08	0.394	78.9
λ_3	0.249	28.62	0.399	71.6

In Table 3, we run the nonlinear energy code, not for the numerical wavetank solution, but for the single sinusoid and it's associated linear potential, given by Equations (1) and (8). This provides a validation of the algorithm and gives us an indication of the error involved in the linear energy estimate, given by Equation (12), which results from using Equation (7) to calculate the kinetic energy, where the integration is taken only up to $\eta = 0$. In contrast, our nonlinear energy estimate continues the integration (numerically) up to η, using Equation (16). Note that this is the only difference between the linear and nonlinear energy estimates for this special case, since the potential energy estimates given by Equations (4) and (15) are identical. Since we have "small amplitude" waves, the two models, linear and nonlinear show very good agreement.

Table 3: $S = 0.02$, $H = 0.0050m$

Type	$\widetilde{\lambda}$	$\overline{E}$	$\widetilde{T}$	$\overline{P}$
linear	0.250	30.66	0.400	76.6
λ	0.250	30.74	0.392	76.8

In Tables 4, 5, 6, 7 and 9 we run the numerical wavetank model for finite amplitude waves with increasing steepness, $S = 0.03, 0.04, 0.05, 0.06$ and 0.07, respectively. It is worth noting that the linear and nonlinear energy estimates show progressively larger differences. This is to be expected since, as the steepness increases the respective nonlinear solution shows an increasing difference in shape from the simple sinusoid shape of the linear small amplitude solution. This involves a raising of peaks and troughs, which would seem to increase the relative potential energy, however, the narrowing of the peaks and broadening of the troughs more than makes up for the raising of the "zero-line". In effect, we have a greater volume of fluid below the still-water level. See [2] . Details of the effect of the KE and PE contributions to the total energy will be presented elsewhere. Again, we here note that since λ_3 is closer to the numerical beach, we expect the energy estimate associated with it to be lower. See Figure (2).

Table 4: $S = 0.03$, $H = 0.0075m$

Type	$\widetilde{\lambda}$	$\overline{E}$	$\widetilde{T}$	$\overline{P}$
linear	0.250	68.98	0.400	172.4
λ_1	0.242	68.8	0.394	174.7
λ_2	0.243	68.6	0.395	173.6
λ_3	0.251	62.75	0.401	156.6

Table 5: $S = 0.04$, $H = 0.010m$

Type	$\widetilde{\lambda}$	$\overline{E}$	$\widetilde{T}$	$\overline{P}$
linear	0.250	122.6	0.400	306.5
λ_1	0.244	118.8	0.395	300.7
λ_2	0.245	118.6	0.396	299.3
λ_3	0.252	108.0	0.402	268.9

Table 6: $S = 0.05$, $H = 0.0125m$

Type	$\widetilde{\lambda}$	$\overline{E}$	$\widetilde{T}$	$\overline{P}$
linear	0.250	191.6	0.400	478.8
λ_1	0.245	180.0	0.396	454.2
λ_2	0.247	179.0	0.397	450.1
λ_3	0.253	162.7	0.402	404.4

Table 7: $S = 0.06$, $H = 0.015m$

Type	$\widetilde{\lambda}$	$\overline{E}$	$\widetilde{T}$	$\overline{P}$
linear	0.250	275.9	0.400	689.5
λ_1	0.247	249.2	0.398	626.5
λ_2	0.250	244.5	0.400	611.4
λ_3	0.251	225.7	0.401	562.8

In Table 8, we run the nonlinear energy code again, not for the numerical wavetank solution, but for the single sinusoid and it's associated linear potential, given by Equations (1) and (8). This provides another validation of the algorithm and gives us an indication of the error involved in the linear energy estimate, given by Equation (12), which results from using Equation (7) to calculate the kinetic energy, where the integration is taken only up to $\eta = 0$. Since we have "finite amplitude" waves, the two models, linear and nonlinear show a slightly larger discrepancy than in the case in Table 3, however, the agreement is still good.

Table 8: $S = 0.06$, $H = 0.015m$

Type	$\widetilde{\lambda}$	$\overline{E}$	$\widetilde{T}$	$\overline{P}$
linear	0.250	275.9	0.400	689.5
λ	0.250	276.7	0.400	691.4

Table 9: $S = 0.07$, $H = 0.0175m$

Type	$\widetilde{\lambda}$	$\overline{E}$	$\widetilde{T}$	$\overline{P}$
linear	0.250	375.5	0.400	938.5
λ_1	0.252	328.3	0.402	817.3
λ_2	0.253	319.7	0.402	794.8
λ_3	0.248	295.1	0.399	740.3

We now compare the total energy $\overline{E}$ for the linear model and total energy $\overline{E}$ for the nonlinear from Tables 1, 2, 4, 5, 6, 7 and 9. In particular, we calculate

$$\text{\%-Difference} = \frac{\left|\overline{E}_{linear} - \overline{E}_{nonlinear}\right|}{\overline{E}_{linear}} \times 100\%, \tag{20}$$

and

$$\text{\%-Of} = \frac{\overline{E}_{nonlinear}}{\overline{E}_{linear}} \times 100\%, \tag{21}$$

where we take the mean of $\overline{E}$ between λ_1 and λ_2, i.e.

$$\overline{E}_{nonlinear} = \frac{\overline{E}_{\lambda_1} + \overline{E}_{\lambda_2}}{2}. \tag{22}$$

Table 10: Comparison of linear and nonlinear total energy.

Steepness	**%-Difference**	**%-Of**
0.01	3.16	103.2
0.02	1.65	101.6
0.03	0.41	99.6
0.04	3.18	96.8
0.05	6.27	93.7
0.06	10.53	89.5
0.07	13.72	86.3

As expected, the percent difference between the linear and nonlinear total energy estimates increases with steepness, up to a maximum of 13.72% for these runs, with maximum steepness, $S = 0.07$. We have no doubt that this difference will only increase with increasing steepness, as the difference between the linear and nonlinear solutions becomes more extreme and as the "small amplitude" assumption in the linear solution becomes more suspect. We noted this earlier in the discussion in this section. We also noted, and offered an explanation for, the observation that the nonlinear estimate is less than the linear estimate as the steepness gets larger. However, we note, with interest that the nonlinear estimate is greater than the linear for very small steepnesses, becoming virtually indistinguishable at steepness, $S = 0.03$. One possible explanation for this, may be the opposing effects of an increase in the nonlinear estimated energy due to the integration "up to the free surface", relative to the linear assumption that $\eta = 0$, and the decrease in the nonlinear estimated energy due to the difference in shape from the simple sinusoid of the linear small amplitude solution. Clearly, these effects must become "momentarily" balanced at steepness, $S = 0.03$.

We end this discussion of Table 10, by noting that the error resulting from the use of simple linear estimates of total energy content over the full nonlinear estimates is present and **significant** even for monochromatic waves. This situation can only become much worse, when we consider the case of more than one component, as in a sea-state simulation.

6 Conclusions

The standard linear ocean energy estimations were reviewed and compared with the estimations using a nonlinear wavetank model for the case of long-crested deep-water monochromatic waves. Our studies showed that the linear model in general over estimates the energy for steep waves, with an error of almost 14% for a 0.07 steepness wave. And this is for the highly idealized case of a single frequency wave. This difference between linear and nonlinear energy estimates for a sea-state, which can be modeled as a spectrum of frequencies, can be expected to be even greater.

A full treatment of the problem, will require an extension of the wavemaker model to finite depth and to three dimensions. Then, the shallow-water and short-crested waves problem, which will invariably arise in evaluating some energy extraction designs, can be studied. Since the wavetank model solves the full potential flow problem, we can perform a complete solution to the problem, including calculation of all accelerations, therefore leading to an estimate of the forces that an energy extraction device may be subjected to.

Acknowledgements

The National Research Council Canada is acknowledged

References

[1] Parsons, W.and Baddour, R.E. (2002) The generation and propagation of transient long-crested surface waves using a waveform relaxation method. *Advances in Fluid Mechanics*

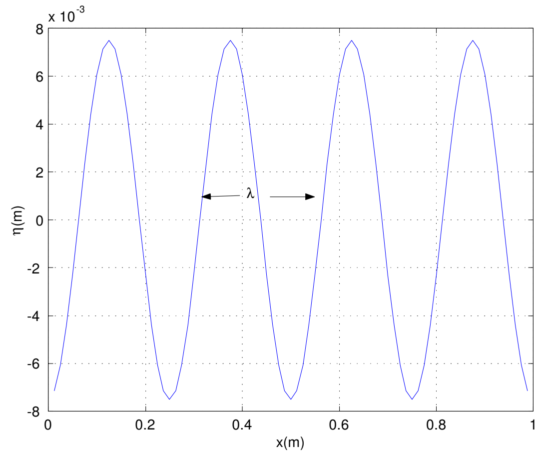

Figure 1: Typical free surface elevation for a sinusoid

2002, WIT Press.

[2] Baddour, R.E. and Parsons, W. (2003) A comparison of Dirichlet and Neumann wavemakers for the generation and propagation of nonlinear, long-crested surface waves. *Proceedings, International Conference of Offshore Mechanics and Arctic Engineering 2003*, Cancun, ASME Paper OMAE2003-37281.

[3] Dean, G.D. and Dalrymple, R.A. (1984) *Water Wave Mechanics for Engineers and Scientists.* Advanced Series in Ocean Engineering, Vol 2, World Scientific.

[4] Baddour, R.E. and Parsons, W. (2004) A comparison of Dirichlet and Neumann wavemakers for the generation and propagation of nonlinear, long-crested surface waves. Journal of Offshore Mechanics and Arctic Engineering, Vol. 126, No 4, 287-296.

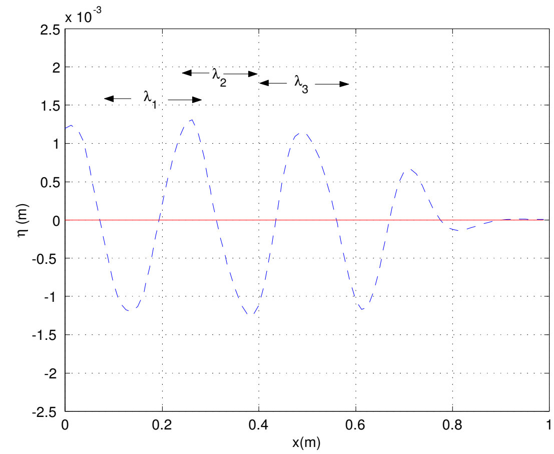

Figure 2: Free surface elevation for numerical wavetank

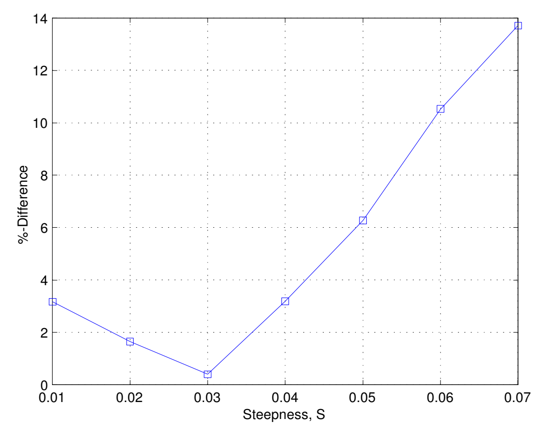

Figure 3: Percent difference vs Steepness

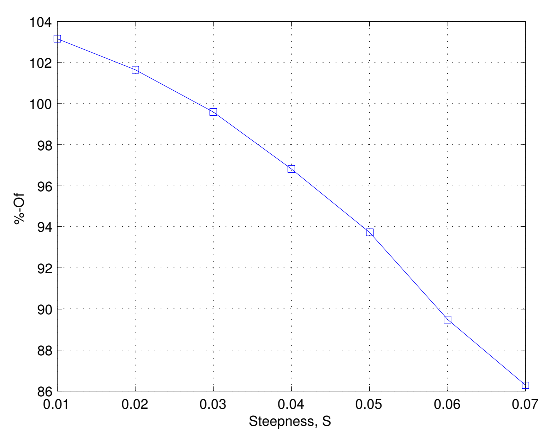

Figure 4: Percent-of vs Steepness